Third International Symposium on Marine Propulsors
smp'13, Launceston, Tasmania, Australia, May 2013

Study on Performance of a Ship Propeller Using a Composite Material

Tadashi Taketani[1], Koyu Kimura[1], Satoko Ando[1], Koutaku Yamamoto[2]

[1]Akishima Laboratories (Mitsui Zosen) Inc, Tokyo, Japan
[2]Mitsui Engineering & Shipbuilding Co., Ltd, Tokyo, Japan

ABSTRACT

Recently, applying a composite material to ship propellers is considered. A phenomenon of the composite material propeller is to deform elastically while a propeller rotating. Using this phenomenon, the design of a new concept propeller which is a high efficiency and reduces a cavitation by adapting to ship wake is studied.

This present paper will describe the composite propeller performances (propeller characteristics and cavitation performance) under the elastic deformation. The several model propellers with the different Young's modulas are made. In order to confirm the propeller characteristics and the cavitation performance of these propellers, the model tests are carried out in a cavitation tunnel of Akishima Laboratories (MITSUI ZOSEN) Inc. The thrust and torque of these propellers deforming elastically are measured, and are compared with the propeller characteristics of a propeller made by aluminum not to deform. And in order to evaluate the cavitation, the fluctuating pressure measurement is carried out in a wake flow simulated by a wire-meshed screen method.

Moreover, the composite propeller is analyzed using FSI (Fluid Structure Interaction) analysis. We will present the comparison between the results of FSI analysis and the model tests results.

Keywords

Composite material propeller, Elastic deformation, FSI

1 INTRODUCTION

Higher fuel costs and pressures to reduce CO_2 emissions are expected to improve ship propulsive performance and fuel efficiency dramatically. Additionally, design changes to improve safety and comfort have increasingly targeted reductions in an accommodation vibration and noise. Propeller cavitations are a major cause of vibrations and noise, and propeller design is expected to move in the direction of minimizing vibration while increasing propulsive performance through higher cavitation performance and efficiency. In recent years, designers have increasingly drawn on composite materials when designing ship propellers to achieve higher efficiency and reduce cavitation through adaptive deformation fitting to non-uniform stern flows.

This paper describes on the results of a study of model propellers characterized by different elasticities. The purpose of the study was to investigate the elastic deformation characteristics of each propeller and the cavitation characteristics caused by such deformation. In applying composite materials to ship propellers, we applied the fluid structure interaction method (FSI) to estimate the propeller characteristics accompanying deformation and to compare model test results to calculated values.

2 MODEL TEST SETUP

2.1 Model Propeller

Model propellers of the same shape but different elasticities were used to evaluate fluid dynamic characteristics and cavitation characteristics attributable to deformation. Table 1 shows the principal particulars for the model propeller; Table 2 describes the properties of these propellers. Dry carbon was the composite material used in this test. We also prepared another test propeller from powders with low Young's modulus (by sintering nylon powders with a laser). We used an aluminum propeller for comparisons and as a reference standard for deformation-free rigid propellers. Figure 1 shows photographs of each propeller.

Table 1 Principal particulars of model propeller

No. of Blade	5
Diameter [m]	0.250
Boss ratio	0.1600
Area ratio	0.4600
Pitch ratio	0.7367
Skew angle [deg.]	20.0

Table 2 Properties of model propellers

	Young's modulus [N/mm^2]	Poisson's ratio
Aluminum	70,000	0.33
Dry-Carbon	51,000	0.34
Nylon Powder	1,240	0.34

(a) Propeller A

(b) Propeller B

(c) Propeller C

(a) Aluminium
(b) Dry Carbon
(c) Nylon Powder

Figure 1 Model propeller

2.2 Test Tank

The model test was carried out in the cavitation tunnel at Akishima Laboratories (MITSUI ZOSEN) Inc, a vertical, high-speed circulating channel. An acrylic window in the measuring section of cavitation tunnel allowed visual observations of model propeller deformation. The tunnel was completely enclosed, making it possible to generate cavitations under controlled water pressures and to observe cavitation during deformation. Figure 2 shows photographs of cavitation tunnel.

Figure 2 Cavitation tunnel

3 PROPELLER CHARACTERISTICS TEST

The propeller dynamometer was arranged in the measuring section of cavitation tunnel and the model propeller was attached to the shaft of the dynamometer. Keeping the number of revolutions of the propeller constant in uniform flow while varying the water flow speed (advance ratio, J), we used the propeller dynamometer to measure propeller revolutions n [sec^{-1}], propeller thrust T [N], and torque Q [Nm]. The analysis assumed a flow speed of Va, as measured with a Pitot tube in the measuring section. The non-dimension values of the measurement results are defined by equations (1)-(4), where ρ is water density, D [m] is propeller diameter.

$$J = \frac{V_a}{nD} \tag{1}$$

$$K_T = \frac{T}{\rho n^2 D^4} \tag{2}$$

$$K_Q = \frac{Q}{\rho n^2 D^5} \tag{3}$$

$$\eta_o = \frac{J}{2\pi}\frac{K_T}{K_Q} \tag{4}$$

Comparison of propellers A (aluminum) and B (dry carbon) were at n=30 [sec^{-1}]. Comparison of propellers A and C (nylon powder) were at n=10 [sec^{-1}], due to strength issues posed by propeller C. Figure 3 show the test results for each propeller. The results indicate lower thrust/torque for propellers B and C compared to propeller A. Propeller C undergoes significant elastic deformation during rotation due to its low Young's modulus, behavior that significantly reduces thrust. Changes in propeller characteristics for propeller B indicate this propeller also underwent to some extent of deformation. In propeller B, the loss of torque exceeded the loss of thrust. As a result, propeller efficiency increased at the same advance ratio J. This suggests the possibility that, even at the same thrust level, the increase in torque is small, while propeller efficiency will improve by to a extent partially determined by changes in deformation-induced characteristics. However, when loss of thrust reaches a certain point, as observed with propeller C at a certain significant level of deformation, propeller performance declines. Deformation has an optimal level.

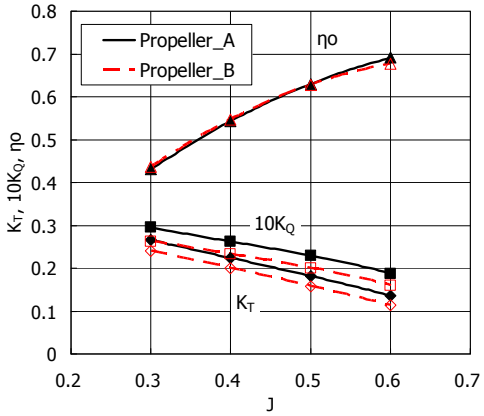

(a) Propeller A and B

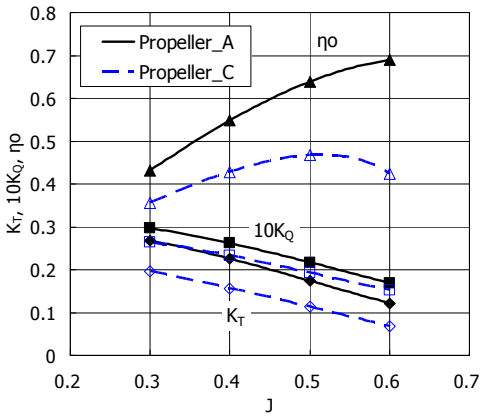

(b) Propeller A and C

Figure 3 Comparison of propeller characteristics

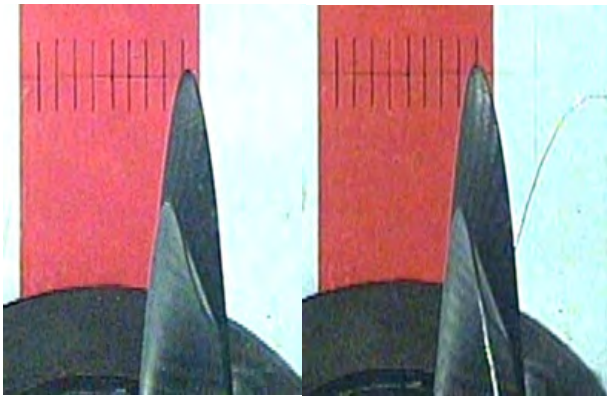

(before) **(after)**

(b) Propeller B

Figure 4 Behavior of deformation (J=0.3)

4 ELASTIC DEFORMATION TEST

Since the propeller characteristics test indicated to some extent of deformation for propellers B and C during rotation, an elastic deformation test was carried out. The propeller blade deformation was observed visually within the plane of propeller rotation by taking instantaneous pictures from points orthogonal to the propeller shaft, matching the propeller revolutions and flash timing, as is commonly done in cavitation tests. The propeller revolutions were set at n=10 [sec^{-1}] for propeller C and at n=30 [sec^{-1}] for propeller B, as in the propeller characteristics test. Table 3 gives the visual inspection results for propeller tip deformation. Figure 4 shows before/after deformation pictures of the propellers (under high load: J = 0.3).

Table 3 Properties of model propellers

Model Propeller	Propeller Revolution [sec^{-1}]	Advance Ratio J			
		0.3	0.4	0.5	0.6
		Tip Deformation [mm]			
C	10	5.4	4.5	3.5	2.6
B	30	1.7	1.8	1.6	1.2

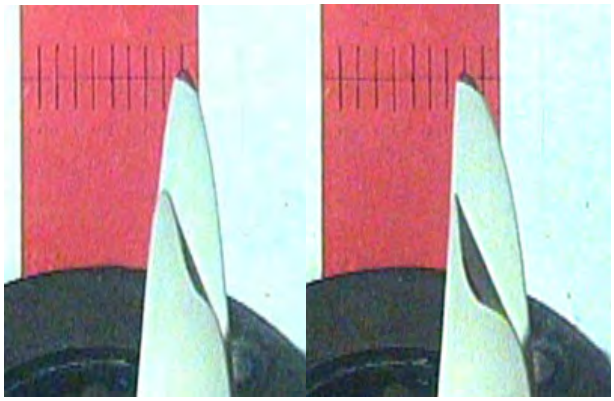

(before) **(after)**

(a) Propeller C

The measurements indicated blade-tip deformations of 3-5 mm in propeller C and blade-tip deformations of 1-2 mm in propeller B. These deformations work as a forward rake. As blade thickness increases from tip to root, the deformation extent increases from root to tip. Deformation at the tip was assumed to account for the major share of deformation effects.

5 CAVITATION TEST

A wire-meshed screen (Figure 5) was arranged in the upstream portion of the measuring section of cavitation tunnel and a non-uniform flow simulating stern wake distribution was generated. In this wake distribution the propeller was allowed to rotate, and the deformation-induced cavitation changes observed. Figure 6 compares cavitation at the same number of propeller revolutions (25.5 sec^{-1}). Cavitation number σn follows equation (5), where Po is a static pressure at propeller position, Pv is a vapor pressure, and σ n = 0.3.

$$\sigma_n = \frac{P_0 - P_v}{1/2\,\rho n^2 D^2} \tag{5}$$

(a) Wire-meshed screen

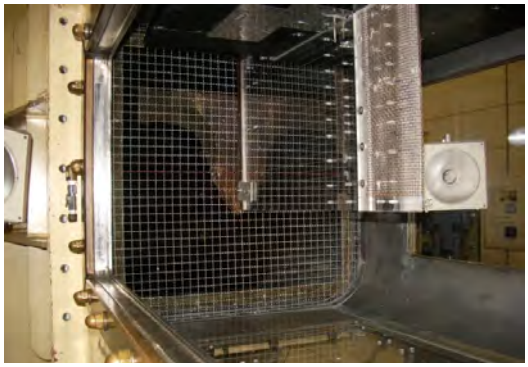

(b) Setup in the measuring section

Figure 5 Wire-meshed screen method

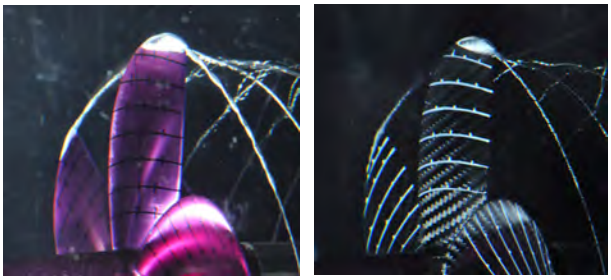

(a) Propeller A **(b) Propeller B**

Figure 6 Comparison of cavitation test results

Test results indicated that volume of sheet cavitation at the blades is less in propeller B than in propeller A and that the tip vortex cavitation also weakens, meaning loads are lower at the blade tip. Presumably, the elastic deformation works as a forward rake at the blade tip and the pitch angle to reduce the load near the blade tip.

The pressure sensor was arranged above the propeller to measure the time-series of fluctuating pressure. Figure 7 shows the 1st order component of propeller revolution number analyzed by FFT. Declining sheet cavitation also reduces fluctuating pressure. When the propeller deforms to reduce loads, cavitation is also reduced, along with fluctuating pressure.

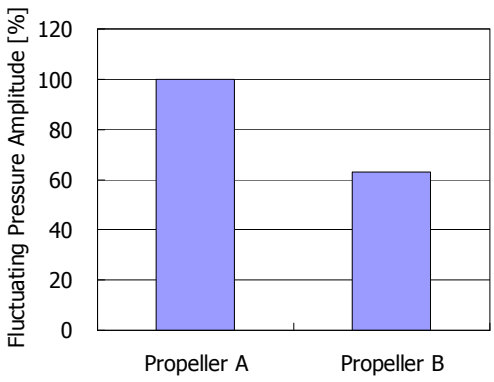

Figure 7 Comparison of fluctuating pressure (1st order)

6 FSI ANALYSIS

Described below is a simulation based on FSI (the fluid structure interaction method). FSI is an analytical tool integrating fluid analysis and structural analysis to estimate the fluid characteristics of an object that deforms in a fluid. In this study, STAR-CCM+ Ver.7.02 was used for fluid analysis and ABAQUS Ver.6.11 was used for structural analysis. Calculation condition assumed J = 0.3, where propeller loads in the propeller characteristics test were greatest. This analysis was performed by the 2-way coupled method (Figure 8).

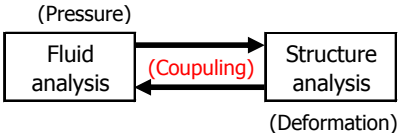

Figure 8 2-way coupled analysis

The analysis proceeded as follows:

1) Apply fluid analysis to calculate pressure distributions at the blade surface.
2) Use structural analysis data as load conditions.
3) Calculate deformation by structural analysis.
4) Morph the fluid analysis mesh based on deformation data.
5) Return to step 1) and perform fluid analysis.

Steps 1–5 were performed iteratively until residual errors in deformation and propeller characteristics were negligible. Figure 9 shows the calculation domains and analysis mesh for the fluid analysis. Since a propeller rotating in a uniform flow has n-fold symmetries equal to the number of propeller blades, calculation was performed with a steady analysis for one blade based on cyclic boundary conditions. In the structural analysis, the mesh was set in a solid model for one blade and was performed with a static analysis under constraining the root of the propeller blade to the propeller boss.

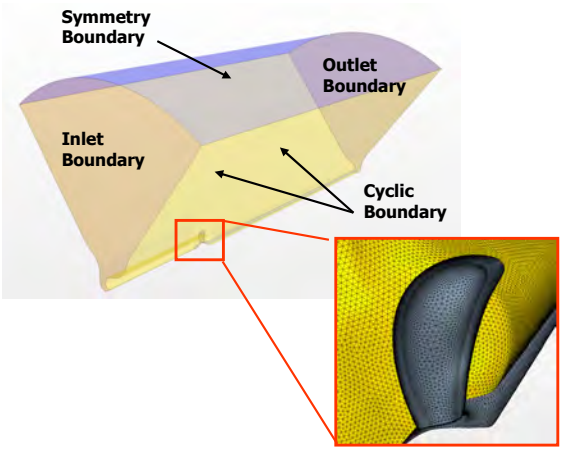

Figure 9 Calulation domains for fluid analysis

Figure 10 shows the propeller characteristics and the maximum deformation at the blade tip along the axis of propeller thrust at each morphing (coupling) of the fluid analysis mesh. Although propellers B and C had different elasticities and different deformations at the blade tip, the parameters converged after approximately the 4th coupling.

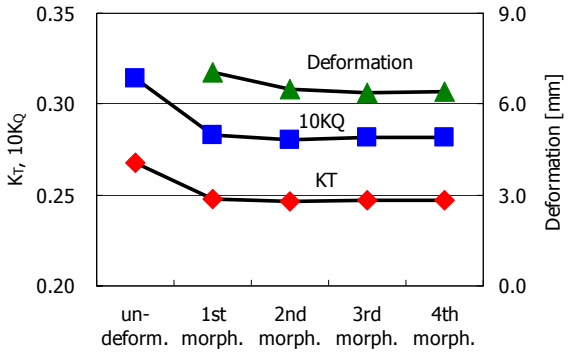

(a) Propeller C

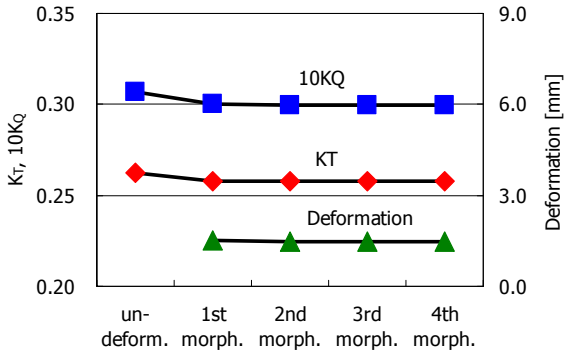

(b) Propeller B

Figure 10 Convergence situation of 2-way analysis

Figure 11 shows the deformation calculation results obtained after the 2-way coupling converges. Both propellers B and C exhibit deformation at the blade tip along the axis of thrust(+), the same results obtained in the model test.

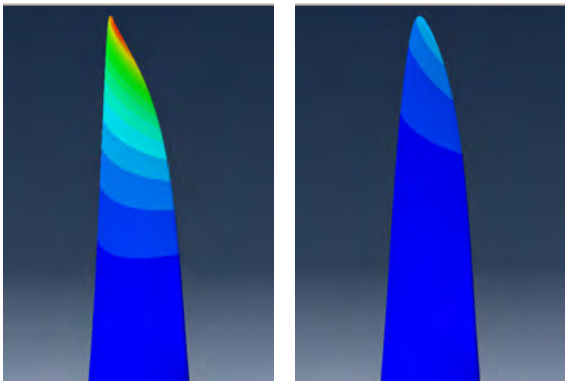

(a) Propeller C **(b) Propeller B**

Figure 11 Deformation calculation results

Figure 12 compares changes in propeller surface pressure distributions before and after deformation. In both propellers B and C, the reduction in pressure at the blade surface is weakened around the blade tip. This effect reduces cavitation volume. The results match those obtained in the cavitation test.

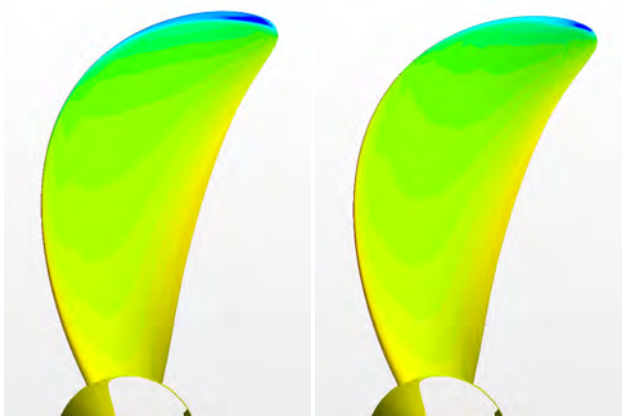

(before) **(after)**

(a) Propeller C

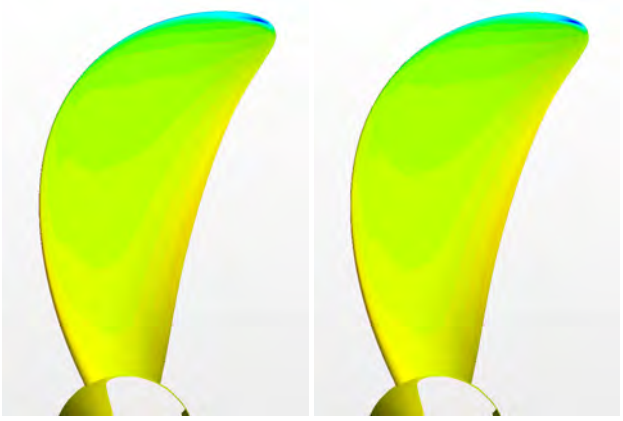

(before) **(after)**

(b) Propeller B

Figure 12 Pressuer distribution before/after deformation

Figure 13 compares the results of model test and calculation for propeller characteristics and deformation. The calculated deformation means maximum deformation along the rotation axis at the blade tip. This figure shows lower thrust/torque after deformation in propeller B but improved propeller efficiency. These results are consistent with the model test results, and estimates of the extent of deformation proved accurate. For propeller C, the deformation itself can be estimated relatively well, but the estimation accuracy of the propeller characteristics after deformation is not sufficient. Where the whole propeller deforms significantly, accurate estimates of the deformation of the whole propeller remain problematic, an issue that remains to be solved.

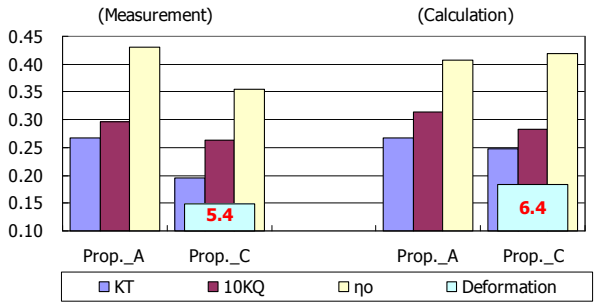

(a) Propeller C

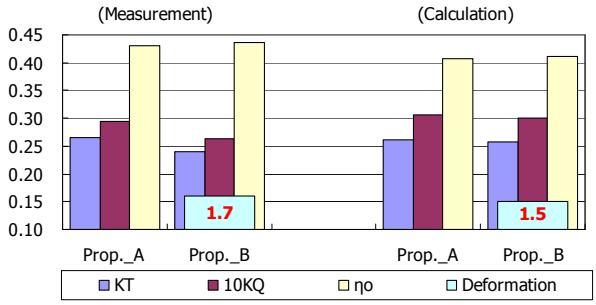

(b) Propeller B

Figure 13 Comparison of the results of model test and calculation

7 CONCLUSIONS

Using model propellers of different elasticities, changes in propeller characteristics, deformation, and cavitation were observed in a model test.

Generally speaking, deformation reduced propeller thrust/torque. Propeller efficiency increased in cases where this deformation was small, since the loss of torque was greater than the loss in thrust. At a certain point, propeller efficiency begins to decline with greater deformation, suggesting an optimal level of deformation.

Elastic deformation was dominant at the blade tip. This deformation occurred along the direction of thrust and worked as a forward rake.

The cavitation generated after deformation indicated that such deformation reduced loads at the blade tip and affected pitch angles. This deformation is expected a reduction of pressure fluctuations.

In FSI analysis, using the 2-way coupled analysis, calculations results and model test results were compared. In the case of small deformations, analysis results were consistent with changes in propeller characteristics. For larger deformations, analysis proved relatively inaccurate in estimating the deformation of the entire propeller. Future efforts should target improvements in this aspect.

REFERENCES

Georgiev, D. J. & Ikehata, M. (1998). Hydroelastic effects on propeller blades in steady flow. Journal of The Society of Naval Architects of Japan, Vol.184.

Young, Y. L. (2008). Fluid-structure interaction analysis of flexible composite marine propellers. Journal of Fluids and Structures.

Motley, M. R., Liu, Z. & Young, Y. L. (2009). Utilizing fluid-structure interactions to improve energy efficiency of composite marine propellers in spatially varying wake. Composite Structures.

Blasques, J. P., Berggreen, C. & Andersen, P. (2010). Hydro-elastic analysis and optimization of a composite marine propeller. Marine Structures, 23.

Young, Y. L. & Motley, M. R. (2011). Influence of material and Loading uncertainties on the hydroelastic performance of advanced marine propellers, Second International Symposium on Marine Propulsors.

Kimura, K., Taketani, T., Ishii, N. & Fujii, A. (2006). Development of low-excitation and high-efficiency propeller design system. Mitsui Zosen Technical Review No.189.

Taketani, T., Ando, S., Kimura, K. & Yamamoto, K. (2012). Study on cavitation behavior of a composite hydrofoil blade. The 16th Symposium on Cavitation, Kanazawa, Japan.